JOURNAL OF SOLID STATE CHEMISTRY **133,** 501–507 (1997)
ARTICLE NO. SC977517

Synthesis, Structure, and Properties of $BaGe_2$: A Study of Tetrahedral Cluster Packing and Other Three-Connected Nets in Zintl Phases

J. T. Vaughey, Gordon J. Miller,[1] Steven Gravelle, E. Alejandro Leon-Escamilla, and John D. Corbett[1]

Ames Laboratory—DOE and Department of Chemistry, Iowa State University, Ames, Iowa 50011-3111

Received March 3, 1997; in revised form June 18, 1997; accepted June 23, 1997

$BaGe_2$ crystallizes in the $BaSi_2$ structure type; space group *Pnma* (No. 62); $a = 9.078(3)$ Å, $b = 6.829(2)$ Å, $c = 11.653(3)$ Å; $Z = 8$; $R = 0.022$; $R_w = 0.025$ ($I > 3\sigma(I)$) for 542 reflections with $2\theta_{max} = 50^\circ$ measured on a single-crystal diffractometer. Magnetic susceptibility measurements confirm its closed shell behavior (diamagnetic), and electrical resistivity measurements place a lower bound on its room temperature resistivity at ca. 1 m$\Omega \cdot$cm. Lattice energy calculations rationalize the observed packing arrangement of $[Ge_4]^{4-}$ tetrahedra and Ba^{2+} cations, while extended Hückel calculations are utilized to compare the electronic structures of various three-connected nets common to Zintl ions with five valence electrons per atom. © 1997 Academic Press

INTRODUCTION

Using Zintl–Klemm formalisms, the structural motifs of many polar main group element phases can be understood as valence compounds (1). These relatively simple electron counting rules can also highlight potential problems in a structural refinement or the presence of an unknown stabilizing impurity, such as the hydride anion. In the latter case, addition of a stoichiometric amount of the appropriate metal hydride as a reagent and precise lattice constant determination have identified a number of instances where binary phases were, in fact, found to be ternary hydride phases (2). One drawback of Zintl–Klemm formalisms, however, is that they have little relevance to predicting structure, although they can be used to understand a known structure. In many cases, a number of structural choices are available with the same electron count because of the different ways the atoms can be packed or linked together while maintaining the correct local geometry. In this paper, we report the structure and physical properties of $BaGe_2$, a Zintl compound containing $[Ge_4]^{4-}$ tetrahedra. In addition, we compare the observed structure with others containing tetrahedral clusters, as well as with the high pressure form of $BaGe_2$: the $ThSi_2$ structure type (3).

Although $BaGe_2$ was first reported in 1968 and shortly thereafter identified from X-ray powder diffraction data as having the $BaSi_2$ structure type (4), its crystallographic details and physical properties have not been previously determined.[2] These data are of interest for comparison to $BaSi_2$ in light of the recent work by Imai and Hirano on the multiple phase transitions and electronic properties as a function of pressure for $BaSi_2$ (5) as well as by the electronics industry in its efforts to identify metal–semiconductor interface materials. Of these, one of the most promising has been the disilicide $CaSi_2$ (WN_2-type), which under pressure also transforms to the $ThSi_2$ structure type, as has been reported for $BaGe_2$ (6, 7).

EXPERIMENTAL

Synthesis. The general techniques were as previously described (8). All materials were handled in a N_2-filled glovebox that had a moisture level below 0.1 ppm (vol). A single-phase sample of $BaGe_2$ was prepared from a stoichiometric amount of barium (APL, 99.9%) and germanium (Aldrich, 99.999%) sealed into a tantalum container. The reaction vessel was then placed inside a silica jacket, evacuated, and sealed. The reactants were heated to 1000°C, held for 1 day, and slowly cooled to room temperature over a one-week period. The sample was single phase on the basis of Guinier X-ray powder diffraction. This phase was initially identified as a product of a reaction with an overall composition "$NaBaGe_3P_3$" along with Na_3P_{11} and Ba_2GeP_2.

X-ray diffraction. Several silvery, irregular block-like, single crystals from the latter reaction were isolated and

[1] To whom correspondence should be addressed.

[2] During review, we learned of another crystallographic study of $BaGe_2$ (4b).

0022-4596/97 $25.00

sealed into thin-walled capillary tubes. Laue photographs were used to determine which crystal was most suitable for structural determination. Diffraction data were collected at room temperature on a Rigaku AFC6R Rotating Anode Diffractometer with Mo$K\alpha$ radiation. Unit cell constants and an orientation matrix for the subsequent data collection were determined from a least-squares refinement of the setting angles of 25 centered reflections in the range $12^\circ \leq 2\theta \leq 36^\circ$. In total, 1480 reflections were measured for the primitive orthorhombic cell in the $+h, \pm k, +l$ octants with $2\theta \leq 50^\circ$; of these, 1071 reflections were considered observed ($I > 3\sigma(I)$). Analysis of the systematic absences within the data set uniquely indicated the space group to be *Pnma* (No. 62). The similarity of lattice constants and space group to those of $BaSi_2$ led us to use its positional parameters as the initial model for the refinement (9). The structure was refined with the aid of the program package TEXSAN (10). Anomalous dispersion and secondary extinction were taken into account during the refinement. After an absorption correction based on three ψ-scans, DIFABS was used to gain a better absorption correction following an isotropic refinement, as recommended by the authors of the program (11). The data set was averaged and reduced to 780 independent observations ($R_{av} = 4.1\%$ for all data), of which 542 were observed ($I > 3\sigma(I)$). The anisotropic refinement of all atoms resulted in R, R_w values of 2.2%, 2.5% at convergence. The maximum and minimum peaks in the difference Fourier map were 1.0 e/Å^3 (2.2 Å from Ge2) and -1.1 e/Å^3.

The lattice constants of a single-phase sample of $BaGe_2$ were refined by a nonlinear least squares method for 33 lines ($20^\circ \leq 2\theta \leq 60^\circ$) from the Guinier X-ray powder diffraction pattern with silicon as an internal standard. Its orthorhombic lattice constants are $a = 9.078(3)$, $b = 6.829(2)$, and $c = 11.653(3)$ Å, in close agreement with the previous literature reports of Weiss (4) and Bruzzone (12). The calculated X-ray powder diffraction pattern for the structure agreed very well with that observed for this sample.

Relevant crystallographic data are listed in Table 1. The atomic positions and equivalent isotropic displacement values, as well as the anisotropic displacement parameters, are given in Table 2. Important bond distances and angles appear in Table 3. The F_o/F_c data are available from the authors.

Physical property measurements. Measurements of the electrical resistivity and magnetic susceptibility of $BaGe_2$ were carried out on single-phase polycrystalline samples. Magnetic susceptibility measurements were performed with the aid of a Quantum Design MPMS SQUID magnetometer in the temperature range 10–300 K at a field strength of 3T. Owing to the air and moisture sensitivity of this compound, resistivity measurements utilized the microwave-based Q-technique (13).

TABLE 1
Selected Crystallographic Data for $BaGe_2$

FW	282.56
Crystal system	orthorhombic
Crystal size (mm)	$0.4 \times 0.3 \times 0.3$
Space group, Z	*Pnma* (No. 62), 8
Lattice constants[a]	
a (Å)	9.075(3)
b (Å)	6.808(2)
c (Å)	11.644(3)
V (Å^3)	719.39(4)
Density (calc.), g/cm^3	5.216
μ(Mo$K\alpha$), cm^{-1}	269.14
Relative transmission coeff. range	0.739–1.258
Temperature	298 K
Octants, $2\theta_{max}$	$h, \pm k, l, 50^\circ$
Reflections measured	$1480/(1071 : I > 3\sigma)$
R_{ave}, %	4.1 (all data); $(542/780 : I > 3\sigma)$
Largest unassigned densities	1.0 e/Å^3, -1.1 e/Å^3
R/R_w (%)[b]	2.2/2.5
Sec. extinction coeff.	$2.9(2) \times 10^{-7}$
GOF	1.48

[a] From Guinier X-ray powder data, $\lambda = 1.540562$ Å, 298 K.
[b] $R = \sum||F_o| - |F_c||/\sum|F_o|$; $R_w = [\sum w(|F_o| - |F_c|)^2/\sum w(F_o)^2]^{1/2}$; $w = 1/\sigma_F^2$.

RESULTS AND DISCUSSION

The compound $BaGe_2$ represents the second crystallographically characterized example of a compound with the $BaSi_2$ structure type, which consists of four crystallographically equivalent, isolated tetrahedra of germanium

TABLE 2
Atomic Positions and Equivalent Isotropic and Anisotropic Displacement Parameters for $BaGe_2$

Atom	Wyckoff position	x	y	z	B_{eq}[a]
Ba1	4c	0.01468(8)	$\frac{1}{4}$	0.69251(6)	0.49(3)
Ba2	4c	0.84173(8)	$\frac{1}{4}$	0.09395(6)	0.58(3)
Ge1	4c	0.4247(2)	$\frac{1}{4}$	0.0916(1)	0.82(6)
Ge2	4c	0.1946(1)	$\frac{1}{4}$	0.9597(1)	0.62(5)
Ge3	8d	0.1921(1)	0.0634(1)	0.14841(8)	0.69(4)

Atom	U_{11}	U_{22}	U_{33}	U_{12}	U_{13}	U_{23}
Ba1	0.0050(4)	0.0070(4)	0.0065(3)	0.0000(1)	0.0000(3)	0
Ba2	0.0093(5)	0.0061(4)	0.0068(4)	0.0000(1)	0.0002(3)	0
Ge1	0.0037(6)	0.0158(8)	0.0115(7)	0.0000(1)	0.0011(5)	0
Ge2	0.0092(7)	0.0096(7)	0.0048(7)	0.0000(1)	−0.0021(6)	0
Ge3	0.0102(4)	0.0062(5)	0.0099(5)	−0.0018(4)	0.0006(4)	0.0027(5)

[a] $B_{eq} = 8\pi^2 \times \frac{1}{3}[U_{11}(aa^*)^2 + U_{22}(bb^*)^2 + U_{33}(cc^*)^2 + 2U_{12}(aa^*bb^*)\cdot\cos\gamma + 2U_{13}(aa^*cc^*)\cos\beta + 2U_{23}(bb^*cc^*)\cos\alpha]$. $U_{eq} = \exp[-2\pi^2(U_{11}h^2a^{*2} + U_{22}k^2b^{*2} + U_{33}l^2c^{*2} + U_{12}hka^*b^* + U_{23}klb^*c^* + U_{13}hla^*c^*)]$.

TABLE 3
Selected Internuclear Distances in $BaGe_2$ and $[Ge_4]^{4-}$ Cluster Bond Angles from $BaGe_2$

Atom–Atom	Distance (Å)	Atom–Atom	Distance (Å)
Ba1–Ge1	3.653(1) × 2	Ge1–Ge2	2.593(2)
	3.410(2)	Ge1–Ge3	2.553(2) × 2
Ba1–Ge2	3.516(2)	Ge2–Ge3	2.542(2) × 2
	3.404(2)	Ge3–Ge3	2.548(2)
Ba1–Ge3	3.454(1) × 2		
	3.397(1) × 2		
Ba2–Ge1	3.786(2)	Ba2–Ge3	3.533(1) × 2
	3.742(2)		3.484(2) × 2
Ba2–Ge2	3.487(1) × 2		3.557(1) × 2
	3.565(2)		

∠Atom–Atom–Atom	Degrees
Ge2–Ge1–Ge3	59.19(4) × 2
Ge3–Ge1–Ge3	59.86(6)
Ge1–Ge2–Ge3	59.64(4) × 2
Ge1–Ge3–Ge2	61.17(5)
Ge1–Ge3–Ge3	60.07(3)
Ge2–Ge3–Ge3	59.92(3)

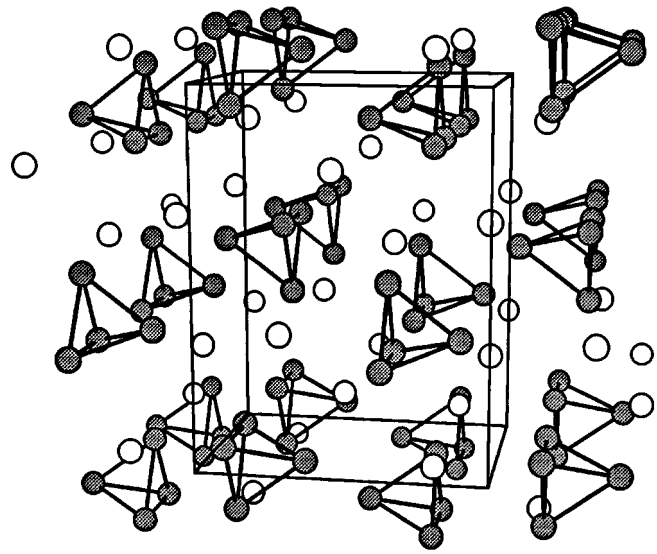

FIG. 1. A clinographic projection of the structure of $BaGe_2$ looking down the [010] direction. The filled circles represent germanium atoms, and the open circles are barium cations.

surrounded by ten Ba cations. A clinographic projection along the [0 1 0] direction is illustrated in Fig. 1. In Zintl cluster chemistry, isolated tetrahedra are one of the more common structural moieties observed for three bonded species ($N = 5$ using the 8–N rule); the other common alternative is a puckered three-bonded sheet, as seen in $EuGe_2$ or elemental antimony. Tetrahedral clusters are the dominant feature in many different structure types, including the Na_2Tl, KGe, NaPb, NaGe, and NaSi structures (14–18). For germanium tetrahedra in particular, Table 4 lists each of the known examples together with a summary of intracluster Ge–Ge bond distances and local point symmetries of the $[Ge_4]^{4-}$ tetrahedra for comparison.

Within these structure types, the germanium tetrahedra all appear to have approximately the same intracluster bond lengths. In terms of the coordination environments, or cation solvation of the $[Ge_4]^{4-}$ clusters, local differences are observed that accommodate the various numbers and types of neighboring cations in each structure type. In CsGe (KGe-type), the four closest Cs cations occupy positions over each face of the tetrahedra for each of the two crystallographically independent clusters (15). These cations are then coordinated at slightly longer distances to the vertices of three neighboring tetrahedra: in total there are 16 Cs cations within 5 Å of each $[Ge_4]^{4-}$ cluster. Furthermore, the cation/anion packing in CsGe produces two short

TABLE 4
Comparison of Bond Distances in Compounds Containing Isolated $[Ge_4]^{4-}$ Tetrahedra

Compound	Structure type: $[Ge_4]^{4-}$ point symmetry		Ge–Ge distances (Å)	Average (Å)	Reference
CsGe	KGe:	T_h	2.591(× 6)	2.591	15
		D_2	2.605(× 2); 2.617(× 4)	2.613	
RbGe	KGe:	T_h	2.574(× 6)	2.574	15
		D_2	2.581(× 4); 2.587(× 2)	2.583	
KGe	KGe:	T_h	2.567(× 6)	2.567	15
		D_2	2.555(× 4); 2.579(× 2)	2.563	
NaGe	NaGe:	C_1	2.537; 2.544; 2.557; 2.578; 2.582; 2.584	2.563	15b, 17
$BaGe_2$	$BaSi_2$:	C_s	2.542(× 2); 2.548; 2.553(× 2); 2.593	2.551	This work

Cs ⋯ Cs contacts of 3.93 and 4.25 Å, versus the average Cs ⋯ Cs distance of 4.75 Å. Nesper and von Schnering have already pointed out that the KGe structure can arise from the NaCl structure by a shift of the anions around certain tetrahedral holes to give a new cubic unit cell ($P\bar{4}3n$) with the cubic cell constant for the KGe-type structure approximately twice the cubic cell constant for the NaCl-type structure, i.e., there are 8 $[Ge_4]^{4-}$ tetrahedra per unit cell (18). The pattern of sites occupied by $[Ge_4]^{4-}$ tetrahedra in CsGe adopts both atomic positions in the asymmetric unit of the A15 (Cr_3Si) structure type.

In NaGe, the single type of tetrahedron has C_1 symmetry (17). Again, there are sodium cations located above each face of the $[Ge_4]^{4-}$ tetrahedron; however, because of the smaller size of a Na cation versus the other alkali-metal cations, the number of cations solvating the cluster is slightly larger (17 Na^+) than in KGe, RbGe, and CsGe (16 K^+, Rb^+, Cs^+) within the same 5 Å distance. This larger number results in a more crowded cation environment around each $[Ge_4]^{4-}$ cluster and gives rise to several competing interactions via sodium packing that appear to lower the point symmetry of the $[Ge_4]^{4-}$ tetrahedron to C_1.

The germanium tetrahedron in $BaGe_2$ is also slightly distorted (site symmetry C_s). Since the structure contains half the number of cations per cluster, the predominant $Ba^{2+} \cdots [Ge_4]^{4-}$ interactions involve face- and vertex-capping as well as edge-bridging of the tetrahedra. This arrangement is shown in Fig. 2. There are two face-capping and five edge-bridging Ba–Ge contacts, as well as four vertex-capping (exo-positioned) Ba cations. The two face-capping barium cations share the same Ge3–Ge3 cluster edge, while the edge-bridging interactions cover the remaining cluster edges, which are between non-crystallographically related Ge sites. From the perspective of the barium cations, Ba1 is bound to six separate $[Ge_4]^{4-}$ tetrahedra in a pseudooctahedral arrangement. Of these interactions, three of the tetrahedra are coordinated along a cluster edge, and three are singly coordinated at vertices. Each Ba2 cation bridges two separate tetrahedra via μ^3 face coordination, two more tetrahedra via μ^2 edge-bridging, and only one cluster is singly coordinated.

Viewing the structure of $BaGe_2$ down the [100] direction reveals a slightly distorted hexagonally close packed array of $[Ge_4]^{4-}$ tetrahedra with one of their pseudo-threefold axes parallel to this unit cell axis. Furthermore, Ba1 cations occupy "octahedral" holes and Ba2 cations occupy one-half of the "tetrahedral" holes in this packing of tetrahedral clusters. The arrangement of Ba1 and Ba2 cations with $[Ge_4]^{4-}$ tetrahedra corresponds to the Co_2Si structure type (space group *Pnma*): According to the classification scheme of Hyde *et al.* ($a/b = 1.33$; $c/b = 1.71$), $Ba_2[Ge_4]$ lies near this field of A_2B structures (19). In order to ascertain why this particular arrangement of $[Ge_4]^{4-}$ tetrahedra arises, we have performed lattice energy calculations (20) on various close-packed arrangements of $[Ge_4]^{4-}$ tetrahedra, in particular those involving hexagonally (hcp) and cubic close packings (ccp). Pólya's theorem (21) helps to enumerate the number of possibilities that exist, but we must establish some constraints on the orientations of the $[Ge_4]^{4-}$ tetrahedra: (i) in ccp, the four threefold axes of each tetrahedron are kept parallel to the threefold axes of the parent cubic cell; (ii) in hcp, one threefold axis is parallel to the *c* axis of the hexagonal cell.[3] In all cases, four is the maximum number of $[Ge_4]^{4-}$ tetrahedra per unit cell. This combinatorial analysis determines five different arrangements for the hcp variations (hcp-I through hcp-V) and three for the ccp variations (ccp-I through ccp-III), see Fig. 3. Two possibilities exist for ccp-I and ccp-II which depend on the sites occupied by one-half the Ba cations. Table 5 summarizes the results of our lattice energy calculations on these different models, which confirm, indeed, that the observed packing arrangement gives the largest lattice energy. Since the lattice energy is the summation of a long-range Madelung term, a short-range Born–Meyer repulsion term, and a van der Waals term (22), the individual entries demonstrate that $Ba_2[Ge_4]$ adopts a structure with the optimal combination of long-range coulomb attractive forces and short-range closed shell repulsions. There are two other hcp

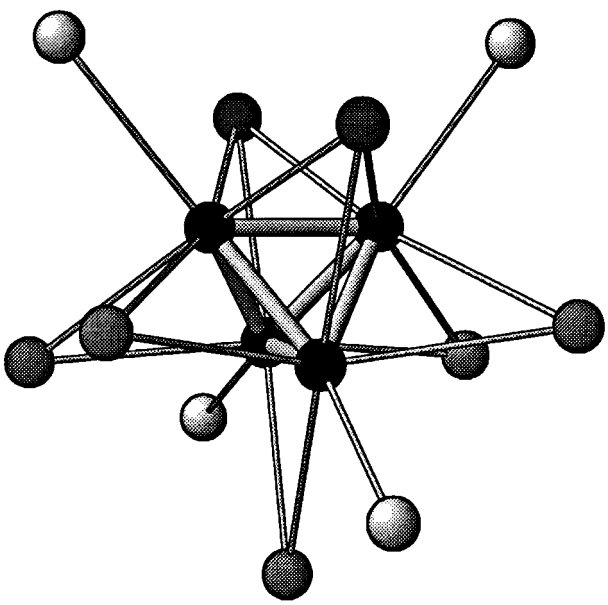

FIG. 2. The local geometry of the $[Ge_4]^{4-}$ tetrahedra in $BaGe_2$. The mirror plane containing the Ge1–Ge2 bond and bisecting the Ge3–Ge3 bond is evident. Face- and edge-bridging Ba atoms are shaded relative to the vertex-capping Ba atoms.

[3] These constraints only affect the individual orientations of each tetrahedron. Once a structure with translational periodicity is constructed, these symmetry elements may, in fact, be lost.

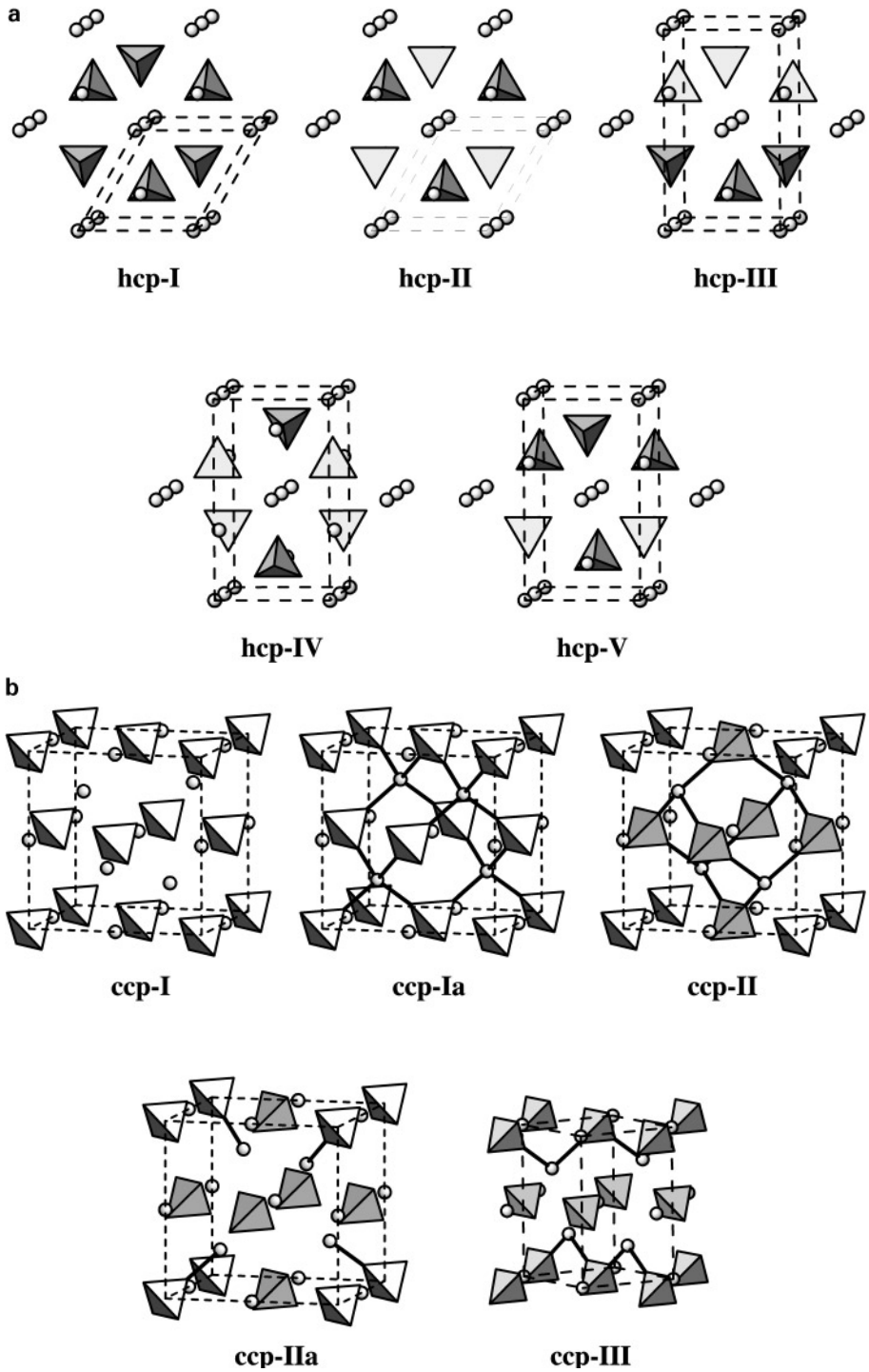

FIG. 3. (a) Hexagonally close-packed structural variants of $BaGe_2$ for lattice energy calculations. The $[Ge_4]^{4-}$ tetrahedra are shown as clusters, and Ba atoms are open circles. Each hcp structure is illustrated down the [001] direction of the hexagonal cell. (b) Cubic close-packed structural variants of $BaGe_2$ for lattice energy calculations. The $[Ge_4]^{4-}$ tetrahedra are shown as clusters, Ba atoms are open circles. Each ccp structure is shown as a clinographic projection with respect to the {100} directions.

alternatives with relatively low lattice energies. Also, the ccp variants with more favorable Madelung energies than the observed structure require such short Ba–$[Ge_4]$ distances ($\sim$2.3 Å) as to produce prohibitively large Born–Meyer repulsions. Among the hcp variants, however, there is very little difference among the calculated lattice energies.

An interesting comparison to the $BaSi_2$-form of $BaGe_2$ is its high pressure structure discovered and studied

TABLE 5
Results from Lattice Energy Calculations on Various hcp and ccp Models of $BaGe_2$

Model	Space group	R_0 (Å)	U_{Mad} (eV)	U_{BM} (eV)	U_{vdW} (eV)	U_{LAT} (eV)
hcp-I	$P6_3mc$	3.01	−18.296	+3.953	−2.700	17.043
hcp-II	$P\bar{3}m1$	3.01	−18.312	+3.952	−2.697	17.057
hcp-III	$Pnnm$	3.01	−18.338	+3.947	−2.675	17.066
hcp-IV[a]	$Pnma$	3.01	−18.349	+3.947	−2.673	17.075
hcp-V	Pm	3.01	−18.324	+3.949	−2.677	17.052
ccp-I	$F\bar{4}3m$	3.67	−15.567	+2.968	−2.626	15.225
ccp-Ia	$F\bar{4}3m$	2.32	−19.687	+11.350	−3.166	11.503
ccp-II	$P\bar{4}3m$	2.32	−18.788	+9.239	−2.996	12.545
ccp-IIa	$P\bar{4}3m$	2.32	−16.728	+5.049	−2.725	14.404
ccp-III	$P\bar{4}m2$	2.32	−18.455	+4.788	−2.663	16.330

Note. R_0 = minimum cation–anion distance; U_{Mad} = Madelung energy; U_{BM} = Born–Mayer repulsion energy; U_{vdW} = van der Waals energy; U_{LAT} = total lattice energy.
[a] Observed structure.

TABLE 6
Results from Extended Hückel Calculations on Various Structural Models of $BaGe_2$

Structure	$\langle E \rangle$ (eV)	q(Ba)	q(Ge)	p(Ge–Ge)	Remarks
AlB_2-type	2.06	0.86	4.57	0.31	Metallic
$BaSi_2$-type	0.00	0.86	4.63	0.42	Nonmetallic
		0.62			
$EuGe_2$-type	0.84	0.88	4.56	0.34	Semimetallic
$SrSi_2$-type	0.38	0.66	4.67	0.41	Nonmetallic
$ThSi_2$-type[a]	0.64	0.96	4.52	0.41	Metallic
$ThSi_2$-Type[b]	1.08	0.78	4.61	0.40	Metallic

Note. $\langle E \rangle$ = total valence electron energy per formula unit relative to the $BaSi_2$-type; q(Ba) = Mulliken population for Ba (there are two sites in the $BaSi_2$-type); q(Ge) = Mulliken population for Ge; p(Ge–Ge) = average overlap population for the Ge–Ge bonds of length 2.55 Å in the structure.
[a] $ThSi_2$-type: Maximum unit cell volume for a fixed Ge–Ge distance of 2.55 Å.
[b] $ThSi_2$-type: All Ge–Ge–Ge angles fixed at 120°.

crystallographically by Evers, Oehlinger, and Weiss (3). At 4.0 GPa and 1000°C, $BaGe_2$ undergoes a transition to the $ThSi_2$ structure type, which consists of a rigid three-dimensional three-connected framework of Ge atoms. The bond distances in the high pressure structure change slightly from the $BaSi_2$-type, going from three equidistant bonds at ca. 2.55 Å to a combination of one at 2.504 Å and two at 2.653 Å. Additionally, each germanium atom remains three-bonded but is now found in a planar coordination. Zheng and Hoffmann attribute this unusual coordination geometry to some double-bond character within the germanium chains (23). Their calculations also point out that the $^3_\infty[Ge^-]$ network produces no energy gap at the Fermi level: it should be a metallic conductor.

We have also utilized extended Hückel calculations (24) to compare $BaGe_2$ in a variety of structures involving three-connected nets of Ge^-: these include AlB_2, $EuGe_2$, $ThSi_2$, $SrSi_2$, and $BaSi_2$. (See the Appendix for details.) In each model, the three Ge–Ge bonds at each Ge site are set at 2.55 Å (the average Ge–Ge distance within the $[Ge_4]^{4-}$ tetrahedron in $BaGe_2$). Table 6 lists the relative total electronic energies per formula unit and Mulliken (atomic) populations for these structural models of $BaGe_2$. There are two entries for the Mulliken populations of the Ba atoms in the $BaSi_2$-type since there are two inequivalent Ba sites in this structure. Figure 4 illustrates how the total electronic energy of the $^n_\infty[Ge^{m-}]$ networks vary with electron count between 4.5 and 5.5 electrons per Ge atom. Near five electrons, the $BaSi_2$- and $SrSi_2$-types are preferred. At lower electron counts, the $ThSi_2$- and $EuGe_2$-types become favored. We surmise that under pressure, less charge transfer occurs from Ba to Ge, which leads to the observed structural preferences. Further theoretical investigations are underway using nonempirical electronic structure methods to study these high pressure transitions.

With respect to the physical properties of $BaGe_2$, a temperature-dependent magnetic susceptibility measurement confirms its closed shell electronic structure, as would be expected for a 20-electron $[Ge_4]^{4-}$ tetrahedral cluster. The result of this measurement, including the addition of a diamagnetic core correction of 4.6×10^{-5} emu/mol, shows the $BaGe_2$ sample to be diamagnetic and to contain ca. 2.2%

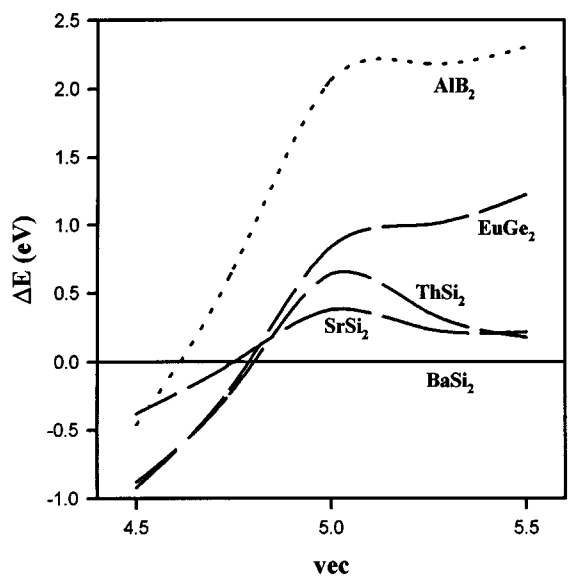

FIG. 4. Total valence electron energy per formula vs electron count for each structure type listed in Table 6 as candidates for $BaGe_2$. The $BaSi_2$-type is the reference ($\langle E \rangle = 0$ eV).

paramagnetic impurities. High frequency measurements gave approximate resistivities of 2.4(8) $m\Omega \cdot cm$ at 260 K and 1.0(3) $m\Omega \cdot cm$ at 100 K. These values are lower than those found in $BaSi_2$ using the four-probe technique (5): ca. $150\,\Omega \cdot cm$ at 260 K and ca. $700\,\Omega \cdot cm$ at 100 K.

CONCLUSION

We have isolated, crystallographically characterized, and studied the properties of the low temperature phase of $BaGe_2$. It adopts the $BaSi_2$ structure type and has similar Ge–Ge distances to those in other compounds containing isolated $[Ge_4]^{4-}$ tetrahedra. Lattice energy calculations rationalize its structure, which can be described as a variation on the orthorhombic Co_2Si structure, i.e., $Ba_2[Ge_4]$, in which $[Ge_4]^{4-}$ tetrahedra occupy the Si sites. In accordance with Zintl–Klemm rules for a closed shell cluster compound, $BaGe_2$ is diamagnetic, but approximate resistivity measurements give values that are 10^{-5} of those for $BaSi_2$. Extended Hückel calculations on several different three-connected networks of Ge^- confirm the preference of the $BaSi_2$-structure type at low pressures, as well as the observed transition to the $ThSi_2$-type at higher pressures.

APPENDIX

The extended Hückel calculations were carried out within the framework of the tight-binding approximation (25). The atomic parameters are as follows: for Ba, 6*s*, $\zeta = 2.14$, $H_{ii} = -7.67$ eV; 6*p*, $\zeta = 2.08$, $H_{ii} = -5.01$ eV; for Ge, 4*s*, $\zeta = 2.16$, $H_{ii} = -16.00$ eV; 4*p*, $\zeta = 1.85$, $H_{ii} = -9.00$ eV. Integrated quantities, e.g., total valence energies, Mulliken populations, and overlap populations, were evaluated by using special *k*-point sets in the corresponding Brillouin zones; the number of points ranged between 50 and 90 points. To compare the total valence electron energy for the different structure types, the unit cell parameters of the models were selected to maintain an equal volume per formula unit (89.92 $Å^3/BaGe_2$ unit) for each. Furthermore, positional parameters were calculated in order to keep all three-bonded Ge–Ge distances at 2.55 Å.

Lattice energy calculations were carried out according to previous reports (21). Atomic parameters for these calculations (26) are $r^{(0)} = 1.60$ Å, $\alpha = 1.56\ Å^3$, $\varepsilon = 7.5\ eV \cdot Å^6$, $p = 8$ electrons for Ba; $r^{(0)} = 1.26$ Å, $\alpha = 7.00\ Å^3$, $\varepsilon = 5.0\ eV \cdot Å^6$, $p = 5$ electrons and for Ge.

ACKNOWLEDGMENTS

This research was supported in part by the Office of the Basic Energy Sciences, Materials Science Division, Department of Energy. The Ames Laboratory is operated for the DOE by Iowa State University under Contract No. W-7405-Eng-82. The authors thank Prof. Robert Jacobson and James Anderegg for maintenance of the diffractometer used in this study and Jerry Ostenson for the magnetic susceptibility measurements on $BaGe_2$. In addition, S.G. thanks the NSF for support under the Summer Solid State Chemistry Program for Undergraduates and Small College Faculty.

REFERENCES

1. (a) E. Zintl, *Angew. Chem.* **52,** 1 (1939); (b) W. Klemm and E. Busmann, *Z. Anorg. Allg. Chem.* **319,** 297 (1963).
2. (a) E. A. Leon-Escamilla and J. D. Corbett, *J. Alloys Compd.* **206**, L15 (1994); (b) E. A. Leon-Escamilla and J. D. Corbett, *J. Alloys Compd.*, accepted; (c) R. W. Henning, E. A. Leon-Escamilla, J.-T. Zhao, and J. D. Corbett, *Inorg. Chem.* **36,** 1282 (1997).
3. J. Evers, G. Oehlinger, and A. Weiss, *Z. Naturforsch. B* **35,** 397 (1980).
4. (a) A. Betz, H. Schafer, A. Weiss, and R. Wulf, *Z. Naturforsch. B* **23,** 878 (1968); (b) R. Kröner, Dissertation, Universität Stuttgart, Germany, 1989.
5. M. Imai and T. Hirano, *J. Alloys Compd.* **224,** 111 (1995).
6. (a) S. Fahy and D. R. Hamann, *Phys. Rev.* **41B,** 7587 (1990); (b) T. Hirano, *J. Less-Common Met.* **167,** 329 (1991).
7. J. Evers, G. Oehlinger, and A. Weiss, *J. Solid State Chem.* **20,** 173 (1977).
8. J.-T. Zhao and J. D. Corbett, *Inorg. Chem.* **34,** 378 (1995).
9. H. Schafer, K. H. Janzon, and A. Weiss, *Angew. Chem. Int. Ed. Engl.* **2,** 393 (1963).
10. TEXSAN, Version 6.0. Molecular Structure Corp., The Woodlands, Texas, 1990.
11. N. Walker and D. Stuart, *Acta Crystallogr., Sect. A* **39,** 158 (1986).
12. G. Bruzzone, *Atti Della Accad. Naz. Lin.* **48,** 235 (1970).
13. (a) J. Shinar, B. Dehmer, B. J. Beaudry, and D. T. Peterson, *Phys. Rev. B* **37,** 2066 (1988); (b) S. C. Sevov and J. D. Corbett, *Inorg. Chem.* **31,** 1895 (1992).
14. D. A. Hansen, J. F. Smith, *Acta Crystallogr.* **22,** 836 (1967).
15. (a) E. Busmann, *Z. Anorg. Allg. Chem.* **313,** 90 (1961); (b) J. Llanos, Dissertation, Universität Stuttgart, Germany, 1983.
16. R. E. Marsh and D. P. Showmaker, *Acta Crystallogr.* **6,** 197 (1953).
17. J. Witte and H.-G. von Schnering, *Z. Anorg. Allg. Chem.* **327,** 260 (1964).
18. (a) H. G. von Schnering and R. Nesper, *Z. Kristallogr.* **162,** 202 (1983); (b) R. Nesper, *Prog. Solid State Chem.* **20,** 1 (1990).
19. B. G. Hyde, M. O'Keeffe, W. M. Lyttle, and N. E. Brese, *Acta Chem. Scand.* **46,** 216 (1992).
20. J. Lin and G. J. Miller, *J. Solid State Chem.* **113,** 296 (1994).
21. (a) W. S. Burnside, "Theory of Groups of Finite Order," 2nd ed. Dover Publications, New York, 1955; (b) C. L. Liu, "Introduction to Combinatorial Mathematics." McGraw-Hill, New York, 1968; (c) D. H. Rouvray, *Chem. Rev.* **3,** 355 (1974); (d) T. J. McLarnan and P. B. Moore, *in* "Structure and Bonding in Solids," Academic Press, New York, 1981, Vol. 2 (M. O'Keeffe and A. Navrotsky, Eds.), p. 133.
22. F. Seitz, "The Modern Theory of Solids," Chap. 2. Dover Publications, New York, 1987.
23. C. Zheng and R. Hoffmann, *Inorg. Chem.* **28,** 1074 (1989).
24. (a) R. Hoffmann and W. N. Lipscomb, *J. Chem. Phys.* **36,** 2179, 3489 (1962); (b) R. Hoffmann, *J. Chem. Phys.* **39,** 1397 (1963); (c) J. H. Ammeter, H.-B. Bürgi, J. C. Thibeault, and R. Hoffmann, *J. Am. Chem. Soc.* **100,** 3686 (1978).
25. M.-H. Whangbo, R. Hoffmann, and R. B. Woodward, *Proc. R. Soc. London, Ser. A* **366,** 23 (1979).
26. (a) J. E. Mayer, *J. Chem. Phys.* **1,** 270 (1933); (b) J. R. Tessman, A. H. Kahn, and W. Shockley, *Phys. Rev.* **92,** 890 (1953); (c) D. F. C. Morris, *Acta Cryst.* **11**, 163 (1958); (d) S. C. Bevan and D. F. C. Morris, *J. Chem. Soc.* 516 (1960).